Modelling of an Absorption Cycle with a Direct Ammonia Vapor Generator Inside a Concentrating Parabolic Trough Solar Collector

Sitki Berat Celik[1,2], Antonio Lecuona-Neumann[1], Pedro A. Rodriguez-Aumente[1], Antonio Famiglietti[1]

[1] University of Carlos III, Madrid (Spain)

[2] Middle East Technical University, Ankara (Turkey)

Abstract

A desorber-separator for an absorption machine using a parabolic through solar collector has been recently suggested (Lecuona-Neumann et al. 2016). It significantly reduces the complexity and cost of an absorption-cycle based Solar Heating and Cooling facility. A complex flow develops inside the receiver tube: a two-phase, gravity driven and gravity stratified opposite direction currents including boiling of a liquid-solid dissolution, actually NH_3-$LiNO_3$. This mixture is both the heat absorbing medium and the working fluid of the absorption cycle. The comprehension of the mutual interactions between cycle and solar direct desorber is necessary in order to unveil the potential of this innovative layout. In the current work, simplified assumptions of the complexity are suggested and implemented in a mathematical model of its integration with a single-effect absorption cycle. The performance of the proposed design has been investigated. Results indicate the importance of the subcooled length and the improvement obtained with lower mass fluxes.

Keywords: Absorption, Solar cooling, Parabolic Trough Solar Collector

1. Introduction

The most promising sorption cycles from the point of view of sustainability are those converting the solar energy to pump heat, forming part of the so called solar heating and cooling (SHC) technology. Market competiveness seems difficult owing to the nowadays complexity of a purposely designed fully available facility and the variability of the solar energy. It needs storage and/or a backup system for cloudy intervals. With the nowadays technology, a primary circuit of a Heat Transfer Fluid (HTF, typically water or a thermal oil) receives the solar heat and transports it to the storage and/or directly to the absorption machine, implying complexity, cost, bulk and weight. Elimination of any extraneous HTF can be achieved by heating directly the absorption machine working fluid inside the solar collector with the result of a simpler layout. Moreover, the cost of the facility could be amortized faster by supplying solar heat in winter, cold in summer and even producing electricity as a complement when neither cold nor heat are demanded. Moreover, the absorption machine could implement electricity consumption for boosting the solar energy to satisfy the user demand; this way, energy storage could be reduced and even eliminated as well as the backup electrical inverse Rankine cycle machine, such as proposed by (Vereda, et al. 2012; Vereda, et al. 2014).

The refrigerant ammonia is a low impact natural substance. The usage of NH_3-$LiNO_3$ dissolution as the working fluid is a choice of various advantages. It enables eliminating the rectifier in the cycle and thanks to the chemical properties of NH_3 subzero ^oC can be achieved (Wu, et al. 2014). After all, the HTF has been eliminated because the solution directly circulates inside the solar collectors. That avoids an extra heat exchanger, heat transfer fluid, piping, control valves and pumps. According to (Lazzarin and Noro 2018) the energy spent in pumping the HTF could be more than the gain from the whole system. Here, the dissolution pump from the absorption machine can also serve for propelling the working fluid through the solar collector field.

The layout proposed in (Lecuona-Neumann, et al. 2016) uses a set of parabolic trough collectors (PTCs) with an inclination (tilting) towards the Equator. This enables direct refrigerant vapor, in this case NH_3, generation and separation inside the collector receiver tubes, although other types of concentrating linear solar collectors can be used, such as Linear Fresnel Collectors (LFCs). Due to the tilted orientation, the generated vapor and the weak solution leave the tube at either ends. Inside the tube, a non-well studied flow is produced. It is a two-phase, both

doi:10.18086/eurosun2018.04.19 Available at http://proceedings.ises.org

driven and stratified by gravity, flowing at low velocities $\sim 1\,\mathrm{m/s}$ in opposite directions with a boiling liquid dissolution, Fig. 3. The flow might be subcooled or saturated at the inlet, while it is expected to be saturated and boiling downstream. The absorption process can be observed in the subcooled length. (Famiglietti, et al. 2018) simulated the complex physics inside the tube under the steady-state 1D regime and (López, et al. 2017; López, et al. 2018) under 1D transient conditions. In (Lecuona-Neumann, et al. 2016) the heating of the tube was investigated concluding that the heat received by the vapor is negligible in comparison with the heat received by the liquid as a result of the conductivity of the wall and the much higher heat conductance of the liquid flow. Moreover, the heat interchanged at the interphase is also negligible in comparison with the heat received by the descending liquid stream.

Among other issues, in this study, we estimate the undesired length of the subcooled zone in the receiver tube as a result of the thermodynamic cycle functioning and its impact on other performance parameters. The time profile of the production, here only cold production, is highly valuable for its integration with the user demand. For compactness of the paper, here no electric boosting neither electricity production is considered.

Due to high costs and time-consuming nature of experiments, it seems reasonable to start the investigation with a simulation using a physical model of the whole system beforehand, revealing its performance and limitations and propose design parameters. The herewith simulations involve the meteorological data measured in Madrid, Spain, subjected to a Mediterranean continental climate. Four representative clear days have been selected for the four seasons. The characteristic behaviors include COP and capacity of the design, in addition to the subcooled length.

2. Theory

A single effect absorption cycle incorporates two different flows, refrigerant and dissolution (solution from now on), and uses five main heat exchangers, Fig. 1. The absorber and the desorber (vapor generator plus vapor separator) are where the fluids are respectively joining and separating whereas condenser and evaporator are heat exchangers with the refrigerant alone. Beside all, the system is completed with a pump and two expansion valves, for refrigerant and solution which divide the cycle into high and low pressure parts. Due to the fact that adding a solution heat exchanger to the system significantly increases the efficiency, it is highly preferred to do so. A schematic drawing of the machine is demonstrated in Fig. 1.

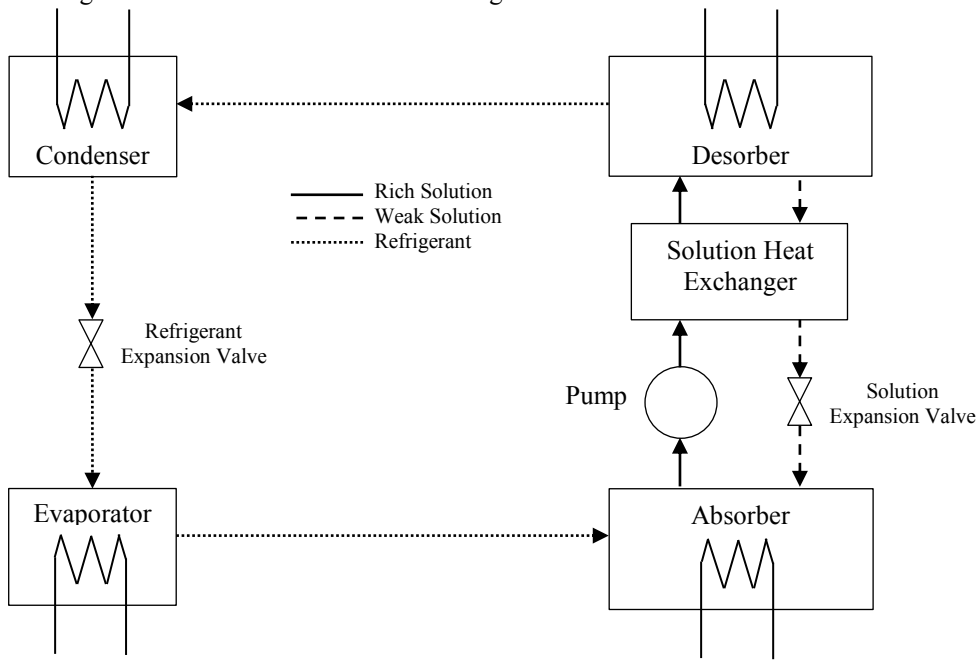

Fig. 1: Single effect absorption cycle

The heat input to the system is through the desorber and the cooling effect is obtained in the evaporator. Heat is rejected from both absorber and condenser. The proposed design replaces the classical desorber and implements a tilted parabolic trough solar collector directly, as shown in Fig. 2. Inside the receiver tube of the parabolic trough

solar collector, the solution is separated into weak solution and refrigerant with the help of heat input by the sun action. The weak solution is in liquid phase whereas the refrigerant is in gaseous phase. Due to tilted position of the tube the liquid is evacuated from the lower exit, as it flows freely, and lets the upper exit of the tube open so that the gas has only the upper exit to leave the tube.

Inside the tube there is a stratified counter-current flow. The liquid solution is driven by gravity and the refrigerant is driven by the evaporation pressure. The low velocities involved assures an almost flat interphase. The solution at the entrance of the tube could be subcooled or saturated with a null quality or positive owing to the performance of the solution heat exchanger. The solution is expected to be saturated at the exit in regular working conditions owing to the effective heat addition as well as for the large contact area with the vapor, small depth as a consequence of the small liquid angle $\varphi < \pi$, Fig. 4, and the turbulent regime experienced.

The cycle has two pressure levels: the condenser, solution heat exchanger and the tube of the parabolic trough contain a high pressure flow, the rest contain a lower pressure flow. As a result, the whole tube has a fairly constant pressure along its longitudinal axis equal to the condenser saturation pressure. The parabolic trough mirror is reflecting the solar radiation uniformly along the tube. However, some portion of it can go to the solution and some other by the refrigerant. That portion varies with the position of the sun, although (Lecuona-Neumann, et al., 2016) explain that the heat fraction going to the vapor flow can be neglected in a first approximation. There, the flowing regime is explained as stratified separated flow with an essentially flat interphase, eventually wavy if a large tilting angle is selected. Possible hydraulic jumps at the exit can be neglected for the purposes of this study.

The mass ratio, Y, of the solution inside the tube is defined as the ratio of the mass flow rate $\dot{m}$ of the dissolved refrigerant ($_r$) to that of the solution ($_s$), both taken > 0.

$$Y = \frac{\dot{m}_r}{\dot{m}_s} \qquad \text{(eq. 1)}$$

Y is decreasing with the amount of separation of refrigerant from the solution when it is flowing downstream along the longitudinal z axis. As a result, the mass ratio at the inlet of the tube is higher of that at the exit. The temperature of the solution T_s is a function of mass ratio Y and pressure P where the former one varies and the latter one is assumed constant along z although a negligible pressure drop is necessary for the vapor upward flow.

$$T_s = f\langle Y, P\rangle \text{ or } T_s \rightarrow T_s\langle z\rangle \qquad \text{(eq.2)}$$

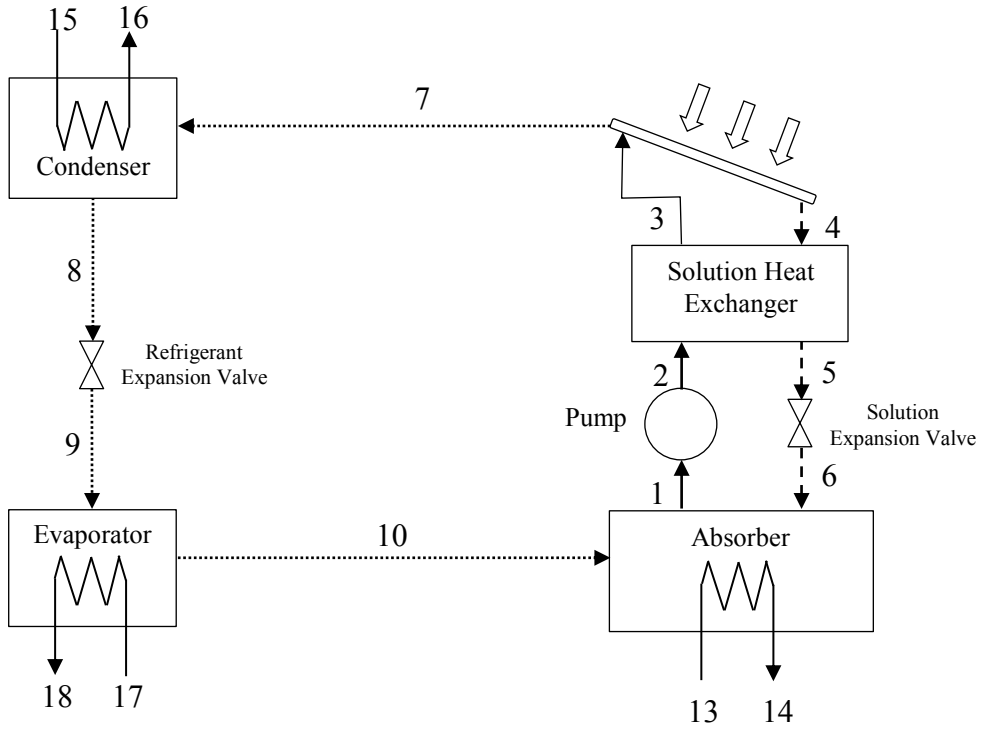

Fig. 2: Proposed design and cycle points nomenclature

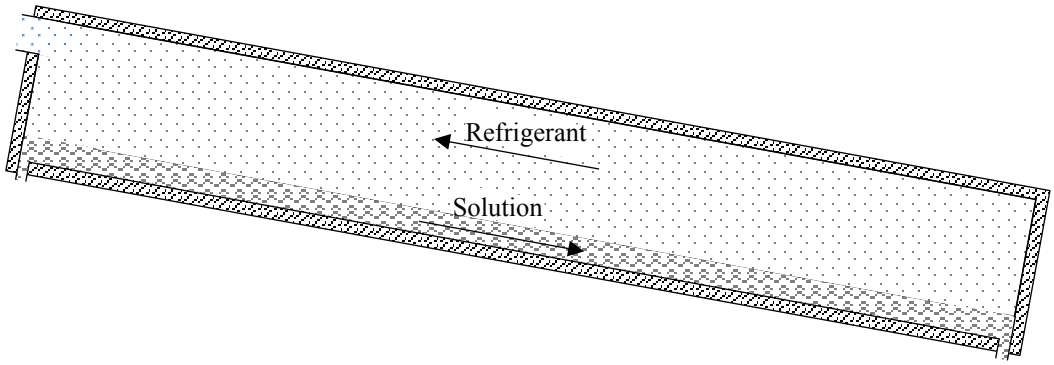

Fig. 3: Fluid flow inside the tube

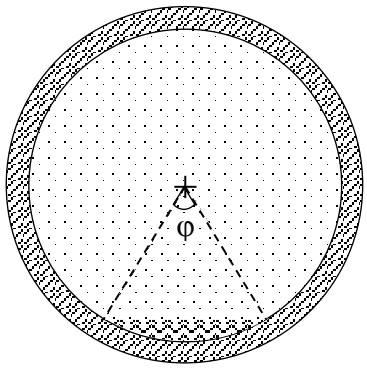

Fig. 4: Cross section of the tube indicating liquid flow angle φ

The bulk flow velocity of refrigerant vapor at the lower end of the tube is null and is increasing toward the upper part as a result of boiling. Even though the refrigerant is generated along the tube, some portion can be absorbed upon meeting a possible subcooled solution at the upper part. The subcooled liquid flow reaches its saturation condition in a lower part of the tube and leaves the tube boiling. Consequently, in the tube, three critical liquid temperatures can be identified; inlet, onset of saturation and exit temperatures where $T_{in} \leq T_{sat} < T_{exit}$. If the solution is already saturated while entering the tube, inlet and saturation temperature for the highest mass ratio are the same. If absorption occurs when the refrigerant meets the subcooled solution, the mass ratio at the inlet and at the onset of the saturation may differ. In Fig. 5 the flow is visualized and Y^- represents the mass ratio at the exit, $Y > Y^-$. Wavy arrows represent the production of refrigerant.

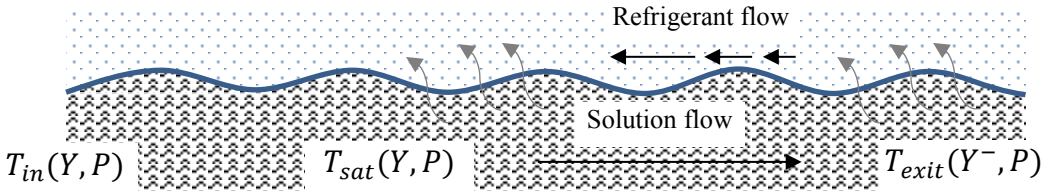

Fig. 5: Critical temperatures for the solution flow

The energy balance of the tube in a 0D representation with either streams perfectly mixed can be formulated as:

$$\dot{H}_s^{in} - \dot{H}_s^{exit} - \dot{H}_r^{exit} + \dot{Q}_{in} - \dot{Q}_{loss} = 0 \qquad \text{(eq. 3)}$$

There, s and r stand for solution and refrigerant respectively. The energy of flow is calculated by their mass flow rates and enthalpies, $\dot{H} = \dot{m}h$, where $h = h\langle T, Y\rangle$. Y is the refrigerant mass fraction of the solution.

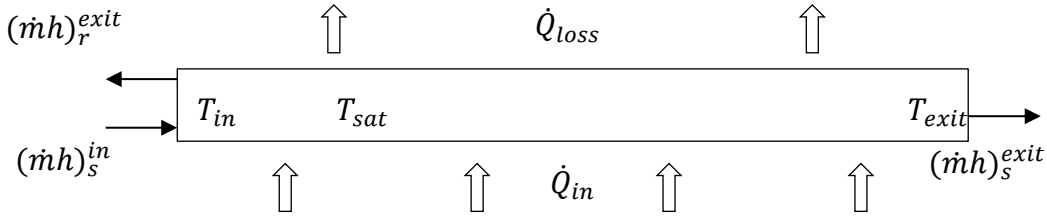

Fig. 6: Heat balance of the tube

Detailed calculation of heat losses is troublesome for such systems due to the complex physics involved. Rather than that, empirical formulas for overall heat transfer coefficients is of common use representing commercial absorber tubes. The overall standardized characteristic equation of the tube estimates the heat losses (ISO, 2017). For a higher accuracy, heat losses are here separated into two distinct zones: Subcooled and saturated. The heat loss formula for a tube of diameter D and length L is:

$$\dot{Q}_{loss} = \pi DL[c_1(T_{ave} - T_a) + c_2(T_{ave} - T_a)^2 + c_3(T_{ave} - T_a)V_{wind}] \quad \text{(eq. 4)}$$

$c_1 = 0.358$ [W m^{-2} K^{-1}]
$c_2 = 0.0019$ [W m^{-2} K^{-2}]
$c_3 = 0.116$ [J m^{-3}K^{-1}]

T_{ave} is the flow average temperature of the zone of interest. T_a is the ambient temperature, V_{wind} is the wind speed. Due to the two different temperature zones, heat losses are calculated separately for those zones of length L_{sub} and L_{sat}.

Mass Balance of the Absorption cycle

The vapor ($_r$) is generated from the rich solution and the remaining is called the weak solution. One has to consider that the amount of salt in the solution does not change. The superscript "-" indicates that the property belongs to the weak solution.

$$\Sigma\dot{m} = 0 \quad \text{(eq. 5)}$$

$$\dot{m}_r = \dot{m}_s - \dot{m}_s^- \quad \text{(eq. 6)}$$

$$\dot{m}_r = x_3\dot{m}_s + Y(1 - x_3)\dot{m}_s - Y^-\dot{m}_s^- \quad \text{(eq. 7)}$$

Where $\dot{m}_r = x_3\dot{m}_s + Y(1 - x_3)\dot{m}_s - Y^-\dot{m}_s^-$(eq. 7) is evaluated at the boundary of the desorber tube. The first term on the right hand side of the equations$Y = \frac{\dot{m}_r}{\dot{m}_s}$(eq. 1) is the contribution of gas phase at the inlet, second term is the amount of the refrigerant in the liquid phase at the inlet and the last one is the refrigerant mass in the weak solution leaving the tube. Note that the inlet condition of the tube can be single phase or two-phase. Which, in other words, means that the solution inlet condition can be subcooled ($_{sub}$) or saturated liquid ($_{sat}$) with quality.

Energy Balance of the Absorption Cycle

The first law of thermodynamics is applied to the individual components of a single effect absorption cycle for steady-state conditions.

$$\Delta H = Q - W \quad \text{(eq. 8)}$$

The detailed form of the first law is demonstrated in Tab. 1 as a set of governing equations, according to the numbering of Fig. 2 where $Lmtd$ is the logarithmic mean temperature difference, v is the specific volume, UA is the thermal conductance and G_{bt} the tilted beam irradiance on the aperture with W_a.

Tab. 1: Application of the first law of thermodynamics to individual components

Component	Equations
Absorber	$\dot{m}_{10}h_{10} + \dot{m}_6 h_6 - \dot{Q}_{abs} - \dot{m}_1 h_1 = 0$
	$\dot{Q}_{abs} = \dot{m}_{13}(h_{14} - h_{13})$
	$Lmtd_{abs} = [(T_6 - T_{14}) - (T_1 - T_{13})]/\ln[(T_6 - T_{14})/(T_1 - T_{13})]$
	$\dot{Q}_{abs} = Lmtd_{abs}\, UA_{abs}$
Pump	$h_2 = h_1 + \frac{W_{pump}}{\dot{m}_1}, W_{pump} = \dot{m}_1 v(P_{high} - P_{low})$
Solution Heat Exchanger	$\dot{Q}_{hex} = \dot{m}_1(h_3 - h_2) = \dot{m}_4(h_4 - h_5)$
	$Lmtd_{hex} = [(T_4 - T_3) - (T_5 - T_2)]/\ln[(T_4 - T_3)/(T_5 - T_2)]$
	$\dot{Q}_{hex} = Lmtd_{hex}\, UA_{hex}$
Solution Expansion Valve	$m_6 h_6 = m_5 h_5$
Desorber Tube	$x\dot{m}_3 h_{3,r} + (1-x)\dot{m}_3 h_{3,s} - \dot{m}_4 h_4 - \dot{m}_7 h_7 + \dot{Q}_{in} - \dot{Q}_{loss} = 0$
	$\dot{Q}_{in} = G_{bT} W_a L_{sub} \eta_{op}$
	$\dot{Q}_{in} - Q_{loss,sub} = m_1 c_p (T_{sat} - T_3)$
	$\dot{Q}_{loss} = \dot{Q}_{loss,sub} + \dot{Q}_{loss,sat}$
	$\dot{Q}_{loss,sub} = \pi D L_{sub}\left(c_1(T_{ave,sub} - T_a) + c_2(T_{ave,sub} - T_a)^2 + c_3(T_{ave,sub} - T_a)V_{wind} \right)$
	$\dot{Q}_{loss,sat} = \pi D L_{sat}\left(c_1(T_{ave,sat} - T_a) + c_2(T_{ave,sat} - T_a)^2 + c_3(T_{ave,sat} - T_a)V_{wind} \right)$
	$T_{ave,sub} = (T_3 + T_{sat})/2\,,\, T_{ave,sat} = (T_{sat} + T_4)/2$
	$L = L_{sub} + L_{sat}$
Condenser	$\dot{Q}_{con} = \dot{m}_7(h_7 - h_8) = \dot{m}_{15}(h_{16} - h_{15})$
	$Lmtd_{con} = [(T_8 - T_{15}) - (T_8 - T_{16})]/\ln[(T_8 - T_{15})/(T_8 - T_{16})]$
	$\dot{Q}_{con} = Lmtd_{con}\, UA_{con}$
Refrigeration Expansion Valve	$\dot{m}_9 h_9 = \dot{m}_8 h_8$
Evaporator	$\dot{Q}_{eva} = \dot{m}_9(h_{10} - h_9) = \dot{m}_{17}(h_{17} - h_{18})$
	$Lmtd_{eva} = [(T_{17} - T_{10}) - (T_{18} - T_{10})]/\ln[(T_{17} - T_{10})/(T_{18} - T_{10})]$
	$\dot{Q}_{eva} = Lmtd_{eva}\, UA_{eva}$

Besides the mass and energy balance equations some complementary equations and assumptions are necessary in order to equate the number of equations to the number of variables. The higher pressure is set to the condensation saturation pressure in the condenser and the lower pressure is set to evaporation saturation pressure in the evaporator. Saturation is also assumed at the exit of the desorber. The refrigerant temperature leaving the desorber tube is assumed to be at the local saturation temperature at the solution exit. The flow regime may be two-phase

depending on the condition at the exit of the expansion valves and at the inlet of the desorber tube (points 6, 9 and 3 respectively in Fig. 2). This condition enables the inlet of the desorber tube to incorporate immediately vapor to the exit stream. As a result, subcooled and saturated flows can be observed inside the whole tube at the same moment.

The simulation requires several input data in two categories. The first one relies on assumptions and the second one relies on measured data. The optical efficiency of the parabolic trough collector is taken to be a constant value, $\eta_{op} = 0.765$ which is a typical value for reflectors with high optical quality (Lovegrove and Stein 2012). Beside those, the length ($L = 3$ m) and aperture area ($LW_a = 3.42$ m^2) of the single PTC and the diameter of the desorber tube ($D = 0.03$ m) are measured data from a real experimental setup. The direct solar irradiance on a 40º tilted, east-west tracking surface and the temperature values are measured data for every 10 minutes on representative days in Madrid, Spain. The solution composes of NH_3 and $LiNO_3$ with equal masses which results in a mass ratio of 0.5. Two test cases have been taken for the mass flow rate of rich solution, 0.01 and 0.02 kgs^{-1}.

The solution in the modelling is a mixture of NH_3 and $LiNO_3$. The thermodynamic properties of the solution are evaluated from Ferreira (Infante Ferreira, 1984) and the refrigerant (NH_3) ones are from Tillner-Roth (Tillner-Roth, et al., 1993). The set of governing equations is non-linear so that an iterative method is used for its resolution. The mathematical tool that is used to solve those equations iteratively at once is called Engineering Equation Solver, EES (F-Chart Software, 2018).

3. Results

In this paper, the simulation runs are oriented to calculate the quasi-steady time evolution of the machine cooling $COP = \dot{Q}_e/\dot{Q}_{in}$, the cooling power $\dot{Q}_e$ and the length of the subcooled zone in the desorber tube L_{sub}. The cycle is cooling down a water stream of 4 ºC inlet constant temperature with a flow rate of 0.6 kg s^{-1}. The representative days are clear days with an average of 1 m/s wind speed. The characteristic values are summarized in Tab. 2. Sunrise and sunset times are the local times. The irradiance is measured for a E-W tracking with 40º constant inclined surface. The irradiation values are plotted in Fig. 7 which the x-axis demonstrates the hour of the day.

Tab. 2: Properties of representative days

	Sunrise	Sunset	Temperature, ºC		Irradiance, kWm^{-2}			Insolation, kWhm^{-2}
			Min.	Max.	Min.	Max.	Ave.	
January	8:50	17:50	5	10	0.10	0.87	0.69	6.09
April	8:20	20:30	11	18	0.10	1.00	0.84	10.09
July	7:40	21:30	22	32	0.10	0.89	0.74	10.13
October	9:10	19:10	14	20	0.10	0.97	0.81	7.90

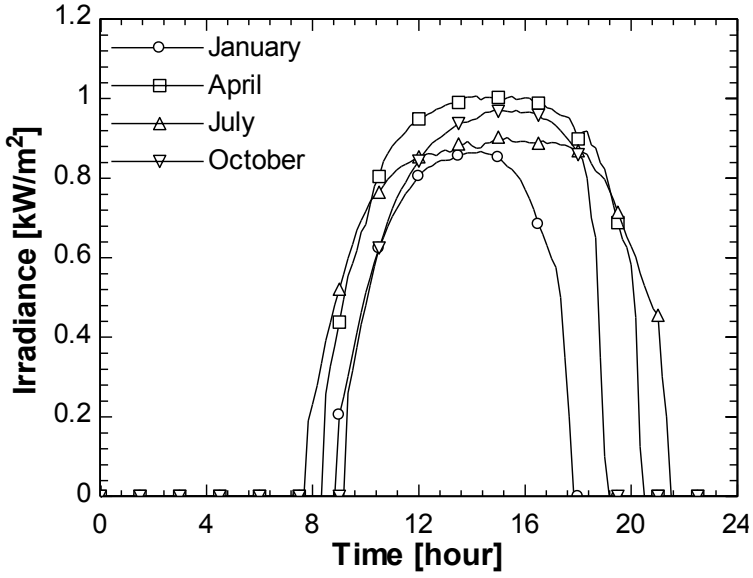

Fig. 7: Daily solar power of the representative days

There are four different days representing four different months with two different mass flowrate conditions through the pump of the cycle. Fig. 8 and Fig. 9 show the COP and cooling power $\dot{Q}_e$ of the cycle for each 10 minutes of the days. The time axes of the plots span between sunrise and sunset which are represented by 0 and 1 respectively. Similarly, 0.5 stands for the solar noon. The plots show that the highest efficiencies are observed in January whereas the highest cooling power is in April. The average COPs and cooling power as well as total cooling energy are summarized in Tab. 3. The average values are calculated from the sunrise to the sunset.

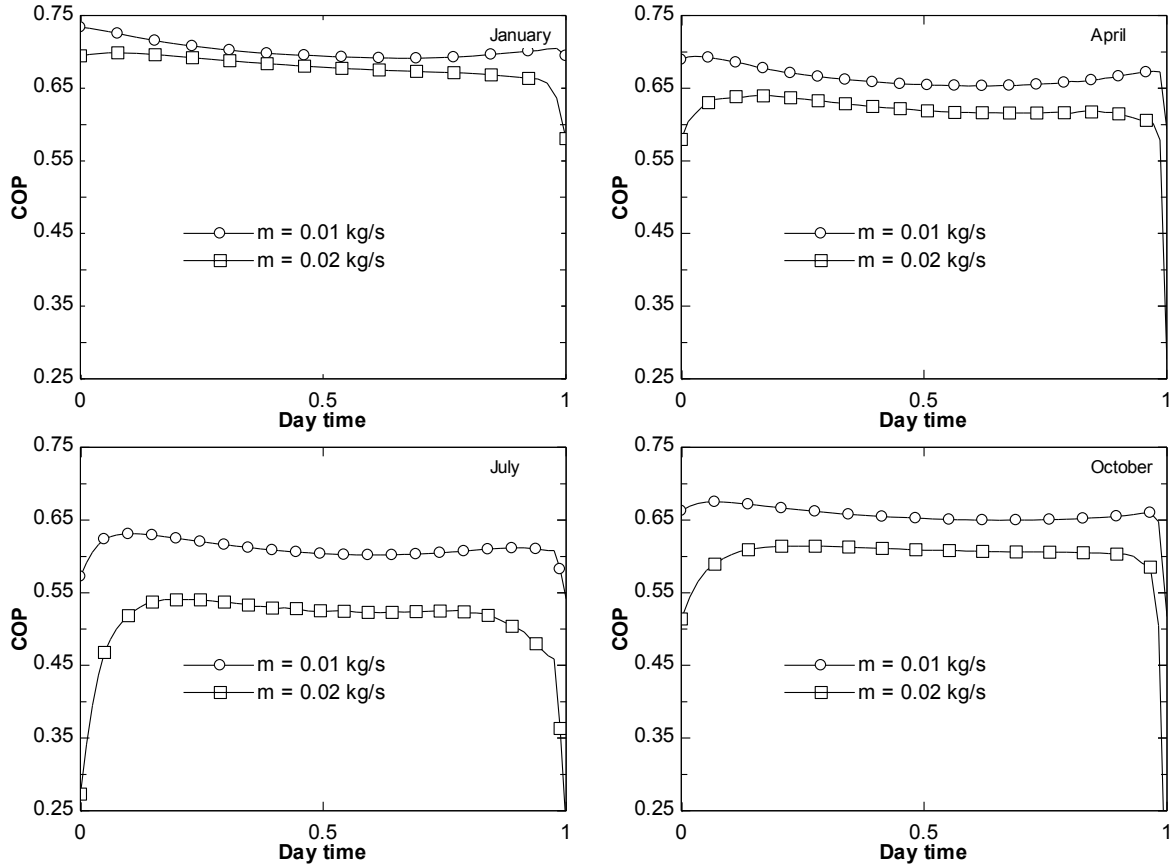

Fig. 8: Time evolution of refrigeration COP along the representative days of each month

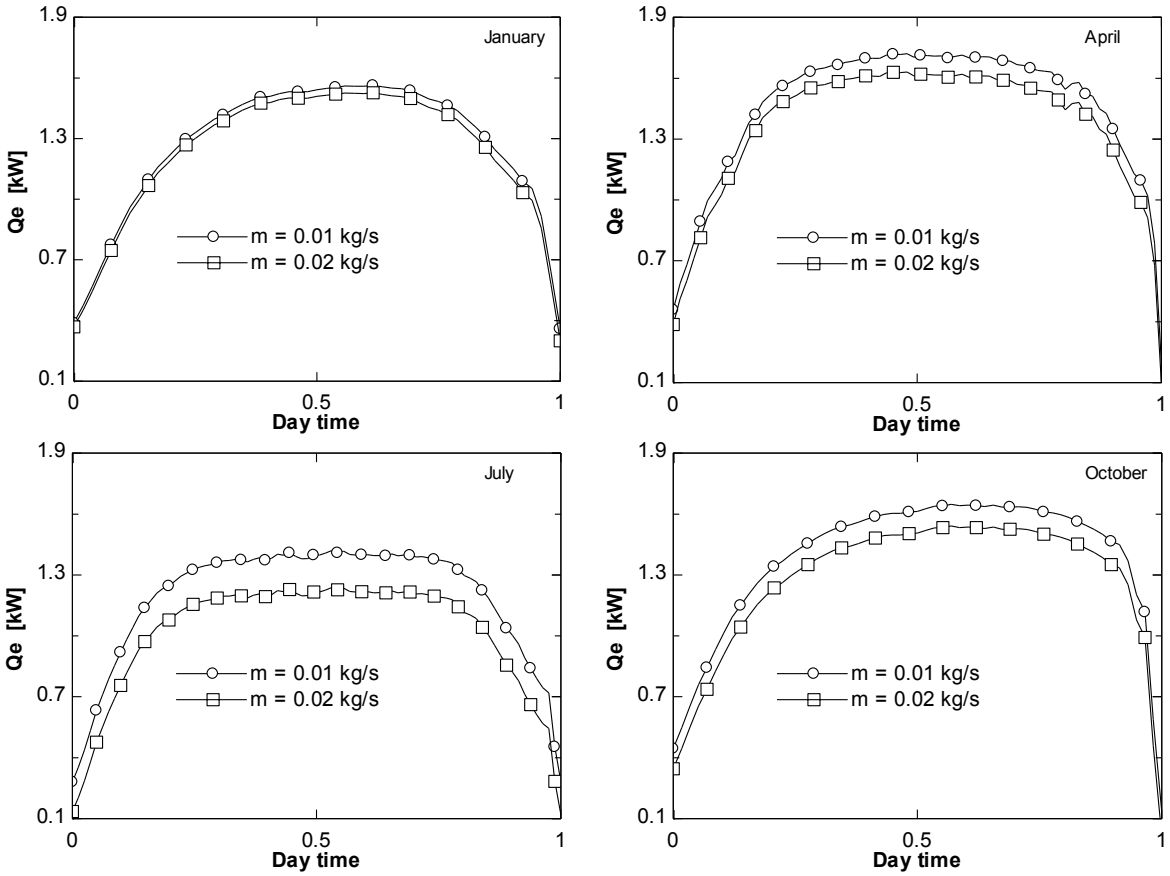

Fig. 9: Time evolution of cooling power $\dot{Q}_e$ along the representative days of each month

Tab. 3: Summary of results

	$\dot{m}$ [kgs^{-1}]	January	April	July	October
Ave. COP	0.01	0.702	0.665	0.610	0.658
	0.02	0.678	0.617	0.508	0.595
Ave. cooling power [kW]	0.01	1.263	1.457	1.182	1.424
	0.02	1.226	1.366	1.007	1.239
Total cooling energy [kWh]	0.01	11.16	17.48	16.15	12.89
	0.02	10.78	16.36	13.74	13.11

The solar integrated cycle reveals that it yields a higher COP and cooling power with the lower mass flow rate of the two ones considered. On the other hand, in terms of COP, the cycle performs better in January than the rest of the months. The reason is that the ambient temperature is relatively lower and hence the high pressure of the cycle is moderated by the lower ambient temperatures. That makes the separation of the refrigerant easier. Also it is worth mentioning that the representative day in January (and each of the others too) is a clear day. Besides performing the highest COP, it has a good average daily cooling power of more than 1.2 kW for $A_a = 3.42$ m^2 PTC. The total heat extracted from the cooling water stream in a whole day has the lowest value despite the high COP and cooling power due to the fact that the day time is lower than the rest of the months studied here. The total cooling energy is calculated by integrating data in Fig. 9 along time. The day in April yields also high COPs compared to the other months and yields the highest cooling power and total energy values. The reason is that the ambient temperatures are still not at the highest levels as in July and the incidence angle to the PTC has the minimum value during this month. The solar panel is east-west tracking but has constant tilt angle of 40 degrees

and located in Madrid at a latitude of 40.333 degrees. The cycle performs the worst values in the July day when the ambient temperatures are the highest and the incidence angle is already high even though there is the highest incoming insolation. The total energy value is fairly good enough thanks to the longer day time in the northern hemisphere. Lastly, the cycle seems to produce fairly good results in October too.

The length where the solution is subcooled, L_{sub}, is plotted in Fig. 10. With a higher mass flow rate $\dot{m}$, it is more likely to have a subcooled zone in the tube. Also, near sunrises and sunsets where irradiance is minimum, the length of the subcooled zone is performing its maximum. In January, due to low internal pressure values, the solution inlet is almost always saturated. In April and October for a mass flow rate of 0.02 kg s^{-1}, the subcooled length L_{sub} is observed to have nonzero values at low irradiance period, yet for the lower mass flow rate it is zero all the time of the days. In July, the subcooled length is calculated to be zero for both flow rates, yet only for the higher flow rate the length is around 0.25 m except near sunrise and the sunset. All in all, apart from sunrise and sunset times, the subcooled length is usually very short. In other words, the solution reaches saturation temperature immediately after entering the desorber tube.

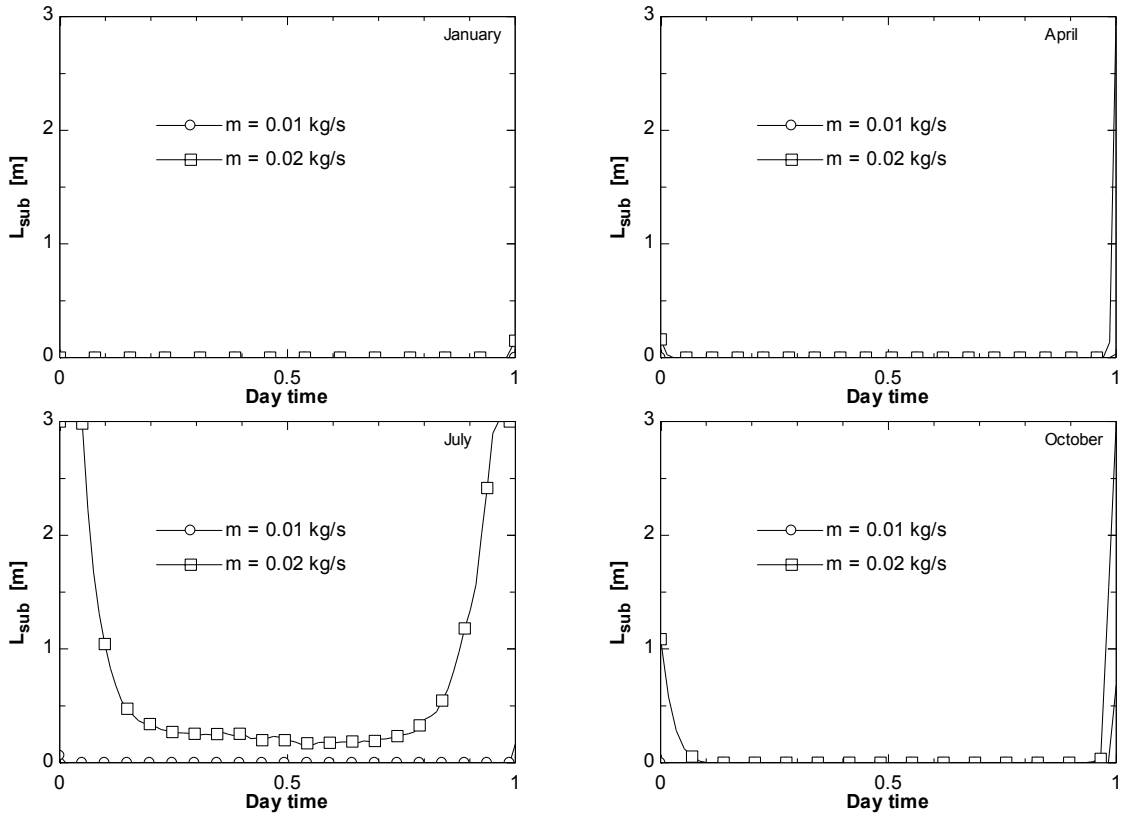

Fig. 10: Time evolution of subcooled zone length L_{sub} along the representative days of each month

4. Conclusions

A single-effect absorption cycle has been integrated with a parabolic trough collector drawing inside it the inner working solution of the absorption machine. That mainly enabled to avoid the HTF and an extra heat exchanger. Also using the solution pair $NH_3/LiNO_3$, the solution rectifier that is necessary for the NH_3/H_2O pair is avoided too. All of those result in an absorption machine with a smaller footprint, lower in price and simpler in design. Besides, that it is placed outdoors makes it safer to use and benefits of not occupying space inside the buildings. The thermodynamic simulation of the absorption machine integrated with the solar collector is performed in order to anticipate the behavior of the proposed design. The simulations are done along four representative days of the four seasons in Madrid, Spain. The PTC is set to be east-west tracking with a constant tilt angle, year-round optimum in this location. The properties of the PTC are taken from a real one and the irradiance and temperature values are measured in Madrid, Spain for clear days. The cycle is set to cool down 4 ^{o}C inlet water stream with a

0.6 kg s^{-1} mass flow rate. The results reveal the cooling COP and cooling power of the absorption machine along the day. A maximum of 0.42 kW m^{-2} of average cooling power has been reached. Also the subcooled length of the desorber tube has been calculated which has a vital role in the performance of the proposed solar integrated cycle. Results show that this length is small for the application data, thus supporting the viability of the technology proposed.

5. Acknowledgements

This work has been partially supported by The Scientific and Technological Research Council of Turkey with the program number 2214/A. The funding of the research project "*Tecnologías energéticas térmico-solares y de aprovechamiento de calores residuales a baja y media temperatura integradas en la red eléctrica*", ENE2013-45015-R from the Spanish *Ministerio de Economía y Competitividad* is greatly appreciated.

6. References

Famiglietti, Antonio, Lecuona-Neumann.Antonio, J. I. Nogueira, and Sitki Breat Celik. "Direct ammonia vapor generation inside a concentrating parabolic trough solar collector for an ammonia/lithium nitrate absorption machine. Theoretical study." Valencia, 2018.

F-Chart Software. 2018. http://www.fchart.com/ees/ (accessed May 21, 2018).

Infante Ferreira, C. A. "Thermodynamic and physical property data equations for ammonia-lithium nitrate and ammonia-sodium thiocyanate solutions." *Solar Energy* 32, no. 2 (1984): 231-236. https://doi.org/10.1016/S0038-092X(84)80040-7

ISO. International Standards Office, Solar thermal collectors -- Test methods. Geneva Patent ISO 9806:2017(en) Solar energy. 2017.

Lazzarin, R., and M. Noro. "Past, present, future of solar cooling: Technical and economical considerations." *Solar Energy*, 2018. https://doi.org/10.1016/j.solener.2017.12.055

Lecuona-Neumann, A., M. Rosner, and R. Ventas-Garzón. "Transversal temperature profiles of two-phase stratified flow in the receiver tube of a solar linear concentrator. Simplified analysis." *ISES.* Palma de Mallorca, 2016. DOI:10.18086/eurosun.2016.04.17.

Lecuona-Neumann, A., R. Ventas-Garzón, Vereda-Ortiz, and M. Legrand. "Linear tube solar receiver as stratified flow vapor generator/separator for absorption machines using NH3/LiNO3." *ISES.* Palma de Mallorca, 2016. DOI: 10.18086/eurosun.2016.04.11

López, R., A. Lecuona, J. Nogueira, and C. Vereda. "Numerical solution of one-dimensional transient, two-phase flows with temporal fully implicit high order schemes: Subcooled boiling in pipes." *Nuclear Engineering and Design*, 2017: 319-329. https://doi.org/10.1016/j.nucengdes.2016.12.027.

López, R., A. Lecuona-Neumann, R. Ventas, and J. Nogueira. "1-D transient numerical modeling of counter-current two-phase stratified flow inside a medium temperature solar linear collector." *Energy Conversion and Management*, 2018: 218-229. https://doi.org/10.1016/j.enconman.2017.10.066

Lovegrove, K., and W. Stein. *Concentrating Solar Power Technology: Principles, Developments and Applications.* 1st Edition. Woodhead Publishing, 2012. ISBN: 9780857096173

Machiels, Olivier, S. Erpicum, B. J. Dewals, P. Archambeau, and M. Pirotton. "Continuous formulation for bottom friction in free surface flows modelling." *WIT Transactions on Ecology and the Environment* 124 (2009): 81-92. doi: 10.2495/RM090081

Tillner-Roth, R, F Harms-Watzenberg, and H D Baehr. "Eine neue Fundamentalgleichung fur Ammoniak." *DKV-Tagungsbericht* 20 (1993): 167-181. ISSN: 0172-8849.

Vereda, C., R. Ventas, A. Lecuona, and M. Venegas. "Study of an ejector-absorption refrigeration cycle with an adaptable ejector nozzle for different working conditions." *Applied Energy*, 2012: 305-312. https://doi.org/10.1016/j.apenergy.2011.12.070.

Vereda, C., R. Ventas, A. Lecuona, and R. López. "Single-effect absorption refrigeration cycle boosted with an ejector-adiabatic absorber using a single solution pump." *International Journal of Refrigeration*, 2014: 22-29. https://doi.org/10.1016/j.ijrefrig.2013.10.010.

Wu, W., B. Wang, W. Shi, and X. Li. "Absorption heating technologies: A review and perspective." *Applied Energy*, 2014: 51-71. https://doi.org/10.1016/j.apenergy.2014.05.027.